DNA 4187F-1

MEASUREMENT OF ISOCHORIC PRESSURE-ENERGY RELATIONS FOR POROUS MATERIALS

Part I—Stress-Matching Technique and Reference Material Results

Ktech Corporation
901 Pennsylvania Ave., N.E.
Albuquerque, New Mexico 87110

30 November 1976

Final Report for Period October 1975—November 1976

CONTRACT No. DNA 001-76-C-0056

THIS WORK SPONSORED BY THE DEFENSE NUCLEAR AGENCY
UNDER RDT&E RMSS CODE B342076464 N99QAXAC03037 H2590D.

Prepared for
Director
DEFENSE NUCLEAR AGENCY
Washington, D. C. 20305

Destroy this report when it is no longer needed. Do not return to sender.

(18) DNA, SBIE (19) 4187F-1, AD-A008 773

UNCLASSIFIED

SECURITY CLASSIFICATION OF THIS PAGE (When Data Entered)

REPORT DOCUMENTATION PAGE

READ INSTRUCTIONS BEFORE COMPLETING FORM

1. REPORT NUMBER: DNA 4187F-1	2. GOVT ACCESSION NO.
3. RECIPIENT'S CATALOG NUMBER	
4. TITLE (and Subtitle): MEASUREMENT OF ISOCHORIC PRESSURE-ENERGY RELATIONS FOR POROUS MATERIALS. Part I—Stress-Matching Technique and Reference Material Results.	5. TYPE OF REPORT & PERIOD COVERED: Final Report [redacted] Oct [redacted] 75—Nov [redacted] 76
	6. PERFORMING ORG. REPORT NUMBER: TR76-11-1
7. AUTHOR(s): N. H. Froula	8. CONTRACT OR GRANT NUMBER(s): DNA 001-76-C-0056
9. PERFORMING ORGANIZATION NAME AND ADDRESS: Ktech Corporation, 901 Pennsylvania Avenue, N.E., Albuquerque, New Mexico 87110	10. PROGRAM ELEMENT, PROJECT, TASK AREA & WORK UNIT NUMBERS: NWED Subtask N99QAXAC30837
11. CONTROLLING OFFICE NAME AND ADDRESS: Director, Defense Nuclear Agency, Washington, D.C. 20305	12. REPORT DATE: 30 Nov [redacted] 76
	13. NUMBER OF PAGES: 58 (54 p.)
14. MONITORING AGENCY NAME & ADDRESS(if different from Controlling Office): KTECH-TR76-11-1	15. SECURITY CLASS (of this report): UNCLASSIFIED
	15a. DECLASSIFICATION/DOWNGRADING SCHEDULE

16. DISTRIBUTION STATEMENT (of this Report)

Approved for public release; distribution unlimited.

17. DISTRIBUTION STATEMENT (of the abstract entered in Block 20, if different from Report)

18. SUPPLEMENTARY NOTES

This work sponsored by the Defense Nuclear Agency under RDT&E RMSS Code B342076464 N99QAXAC30837 H2590D.

19. KEY WORDS (Continue on reverse side if necessary and identify by block number)

Pressure-Energy Relations
Grueisen Stress
Porous Materials
Electron-Beam Testing

20. ABSTRACT (Continue on reverse side if necessary and identify by block number)

For several years pulsed electron beam machines have been used to rapidly deposit energy in sample materials, and various techniques have been employed to infer the resulting constant volume heating pressure-energy (P-E) relation. In Part I, a new electron beam stress-matching technique is described which provides a more direct measurement of both P and E through the utilization of reference materials having known P-E relations. The P-E characteristics of aluminum (6061-T6), germanium (111), quartz (X-cut), and silicon (polycrystal were measured to 100 cal/g and are presented in Part I. The results of the

DD FORM 1 JAN 73 1473 EDITION OF 1 NOV 65 IS OBSOLETE

UNCLASSIFIED

SECURITY CLASSIFICATION OF THIS PAGE (When Data Entered)

408 270

20. ABSTRACT (Continued)

application of this technique to determine the Gruneisen parameters of four porous materials is given in Part II.

PREFACE

This research was sponsored by the Defense Nuclear Agency; the Contracting Officer was Mr. Donald J. Kohler, DNA/SPAS.

The results of this work are presented in two parts. Part I, unclassified, describes the experimental method and presents results for reference materials. Part II, classified, presents the results of applying the stress-matching method to obtain the Gruneisen parameters of porous metals and cermets.

The author was assisted in this work by Mr. E. D. Stretanski and Mr. W. Foreman. During the course of this work, we were aided by technical discussions with Mr. O. Walton and Dr. D. V. Keller.

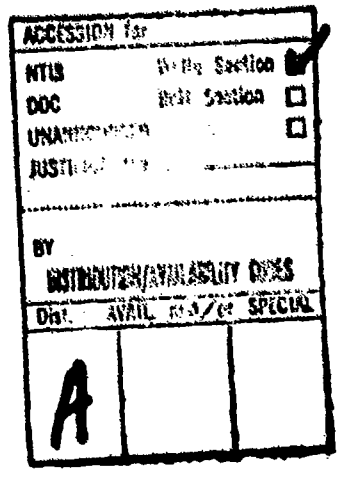

TABLE OF CONTENTS

LIST OF ILLUSTRATIONS

LIST OF ILLUSTRATIONS (Continued)

LIST OF TABLES

CHAPTER 1

INTRODUCTION

The principal objectives of this program were: (1) to develop a technique for the measurement of isochoric pressure-energy relations for solid and porous materials, and (2) to exercise this technique on porous materials, including a metal with two initial densities and two cermets. The former objective is the subject of Part I of this report; the porous material results are presented and discussed in Part II.

For instantaneous energy deposition in a thermoelastic solid the pressure-energy relationship is linear and is defined by the relation

$$P = \gamma \rho E \tag{1}$$

where P is the pressure increase, E is the internal energy change, ρ is the density, and γ is the Gruneisen parameter. Actual energy depositions require a finite time which results in some stress relief and expansion near boundaries; only internal material may have been heated at constant volume. For composite and porous materials the pressure-energy relation is non-linear, and the above expression defines an "effective" Gruneisen parameter which is a function of energy and initial volume. As the internal energy, E, is increased at constant volume in a porous material, the pressure, P, initially increases somewhat proportionally to E; at higher energy the matrix material yields and expands into the voids and there is no further pressure increase (until voids are filled). At even higher energy, the vapor state of the matrix is reached (or the voids become filled) and the pressure increases rapidly with energy. This complex P-E behavior is illustrated in Figure 1. Also shown in Figure 1 is the linear behavior for a selected thermoelastic solid whose slope (Gruneisen) is less than the initial slope for the porous material. At some point (i.e., where the curves cross) the solid and porous materials develop the same pressure for the same change in internal energy. Thus a judicial choice of solid material and internal energy permits matching the porous material stress.

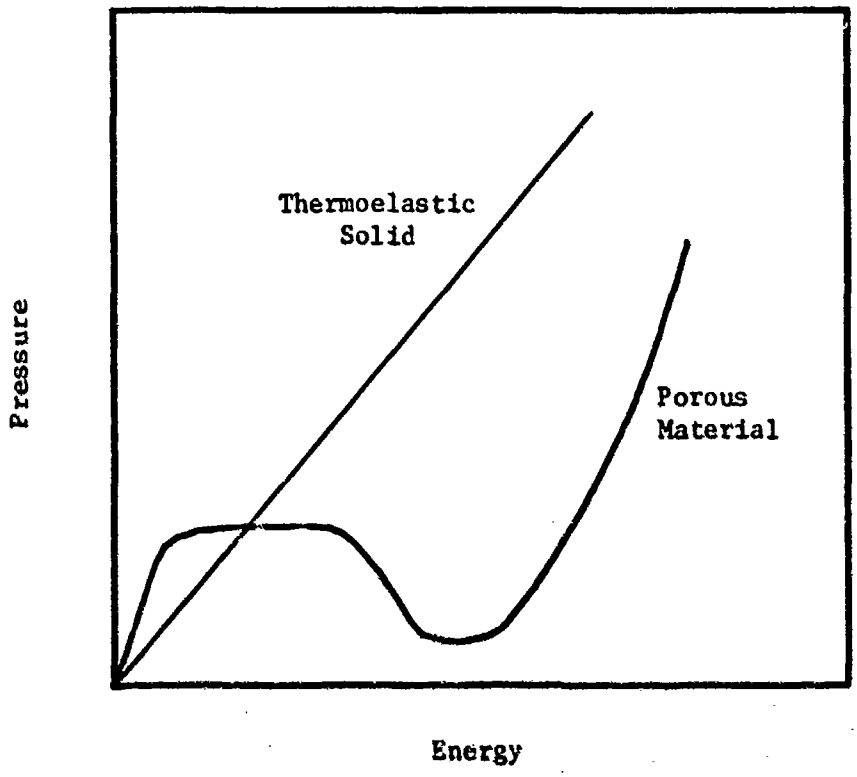

Figure 1. Pressure-Energy Behavior for Solid and Porous Materials

Also of importance is the adiabat centered at the initial pressure-energy state achieved by instantaneous energy deposition at constant volume, as indicated in Figure 2. In general, because Gruneisen measurement experiments involve stress wave measurements, the adiabats are inextricably related to the determination of the initial pressure-energy or Gruneisen state as discussed below.

Most pressure-energy or Gruneisen parameter determinations by electron beam (e-beam) deposition have utilized relatively thick samples; i.e., thick with respect to the electron range. An example of this technique is described by reference 1. The energy gradient in the sample and the finite deposition time result in a poorly defined "initial" pressure-energy state, and in most cases only a small region of the sample is heated at constant volume. A complex material equation of state, a porous material model, and a wave propagation computer code are generally required in order to compute the "initial" pressure-energy distribution from the measured response. The stress attenuation which occurs during wave propagation between the heated portion of the sample through the cold sample to the stress or particle velocity gauge at the rear of the sample limits the resolution of the initial sample pressure and hence the determination of the Gruneisen parameter.

In more recent measurements this situation has been considerably improved through the use of uniformly heated samples utilizing relatively high mean electron energy e-beams and fused silica buffers (see for example, reference 2). The extremely low fused silica Gruneisen parameter results in relatively low stress generation in that material which transmits the stress wave. The fused silica velocity-time profile is measured with an interferometer, or the stress wave is measured with a quartz gauge. The knowledge of the silica adiabats allows a point on the sample expansion adiabat to be directly determined without resorting to complex computer computations; but the adiabatic path joining this point to the initial state is generally not known and must be assumed in order to find the initial (Gruneisen) pressure. The determination of the internal energy change (dose) is also

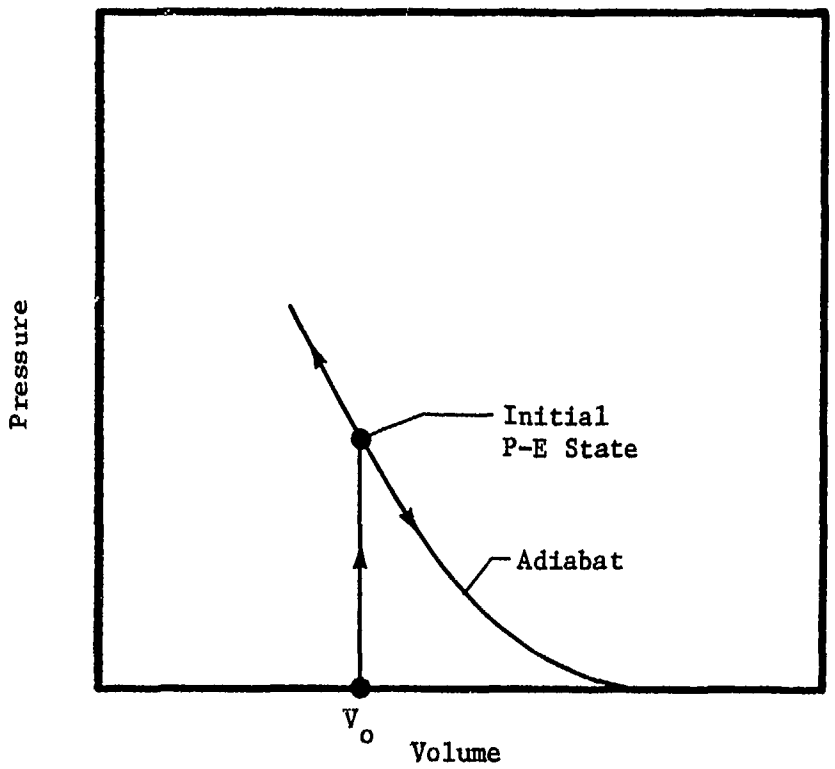

Figure 2. Pressure-Volume Adiabat from Initial Constant Volume State

generally not accurately known because it depends on the electron-beam fluence and depth-dose profile, which in turn depend on calorimetric measurements and machine repeatability.

In the technique utilized in this work, a stress generating reference material replaces the fused silica, and fairly uniform and rapid deposition is desired through both sample and reference material, as indicated in Figure 3. This results in a significant improvement in the ability to determine the initial pressure-energy state. The measured particle velocity-time history at the rear surface of the reference material is characterized by two "steps" of total amplitudes, U_r and U_s, as indicated in Figure 3. Simple analysis, presented in Section 5, allows a point on the sample adiabat close to the initial (Gruneisen) pressure-energy state to be determined from U_r and U_s. The first, or reference step, amplitude determines the internal energy change*, and the second, or sample step, amplitude determines the adiabat point. Several points on an adiabat (both compression and expansion) can be found by utilizing various reference materials while maintaining the same e-beam dose.

The sample pressure is found by a differential technique which compares the reference and sample step amplitudes. In the optimal Gruneisen experiment the sample steps are of equal amplitude (i.e., $U_r = U_s$), implying that the sample Gruneisen stress equals the known reference material Gruneisen stress. This is optimal because when the reference material Gruneisen stress equals the sample Gruneisen stress no extrapolation along the sample adiabat is required. It is clearly desirable to design the experiments so as to minimize the stress differential between sample and reference materials. This new technique will be referred to as the "stress-matching" technique.

---

* It was shown in 1967 (reference 3) that calorimetric e-beam measurements could be made via stress measurements in thermoelastic absorbers.

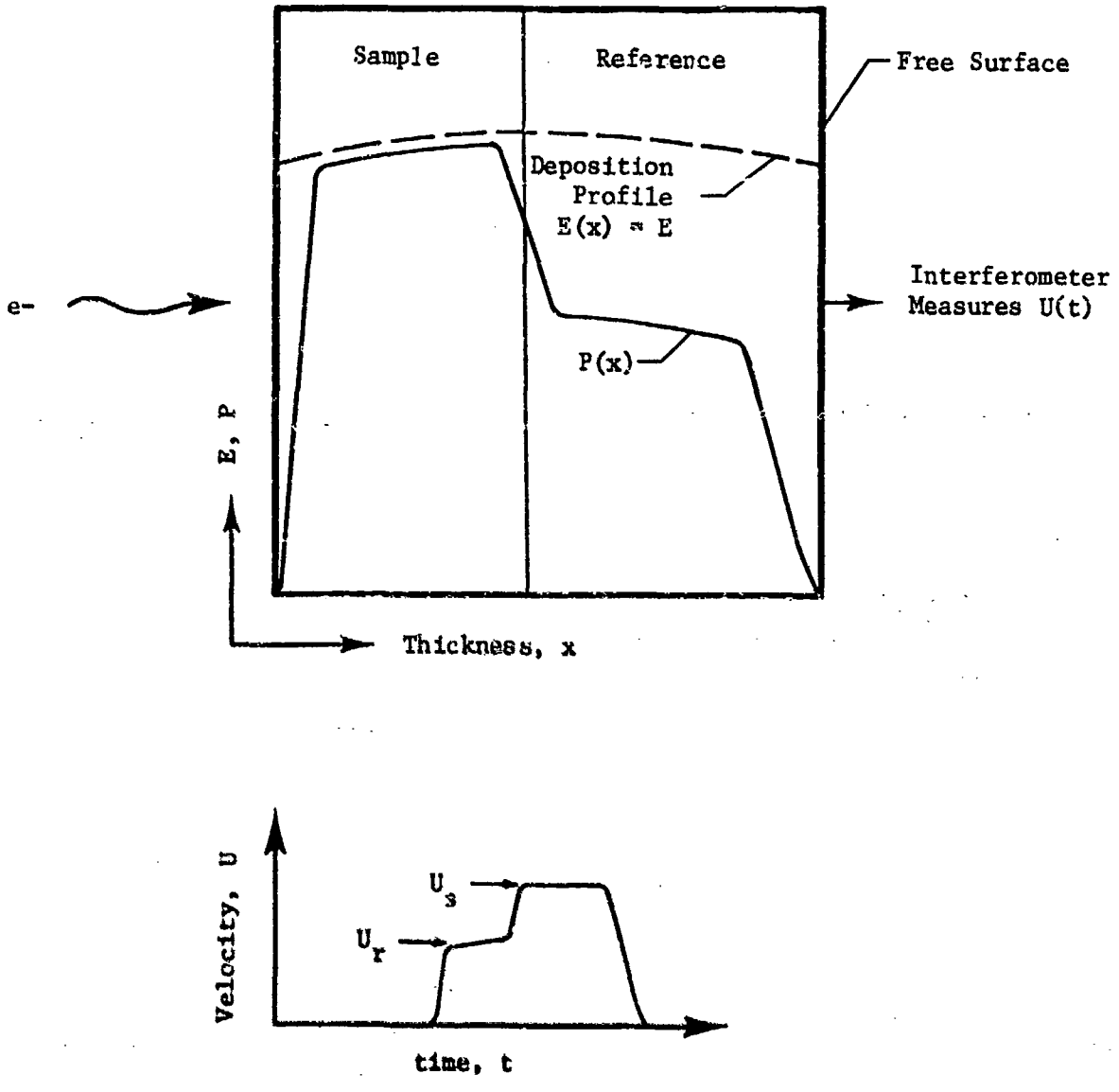

Figure 3. Stress Matching Configuration

CHAPTER 2
EXPERIMENT DESIGN

In order to optimally exercise the "stress-matching" technique introduced above one must select appropriate reference materials and the e-beam machine. These selections are coupled to the thermomechanical properties of each particular sample material; i.e., the same reference materials and electron beam will not provide the optimum experiment for all porous sample materials and dose ranges. However, some general guidelines and procedures for the design of optimal experiments can be given.

The principal requirement for reference materials are: (1) that the material respond in a known and reproducible manner, and (2) that the material's Gruneisen pressure generation (product of Gruneisen parameter and density) for a given internal energy increase (dose) is close to that of the sample to provide a near stress-matching condition. This implies that a number of reference materials are required to characterize a single porous sample material over an energy range. The general validation of the former requirement for a number of reference materials is the subject of Section 6. Candidate reference materials were selected to provide a range of pressure-energy responses in order to satisfy the latter requirement.

Figure 4 indicates the pressure-energy characteristics of the selected reference materials and the range of pressure-energy response anticipated for the porous sample materials (shaded region). The sample pressure will be matched by the various reference materials at the dose levels corresponding to the abscissas at the intersections of the reference and sample response. The reference materials selected were: (1) aluminum (6061-T6), (2) quartz (X-cut), (3) germanium [111], (4) silicon (polycrystaline), and (5) silica (fused).

The e-beam machine choice is based upon meeting the requirements for spatially-wide uniform pressure regions in the sample and reference materials, the response of which produces a well-defined particle velocity

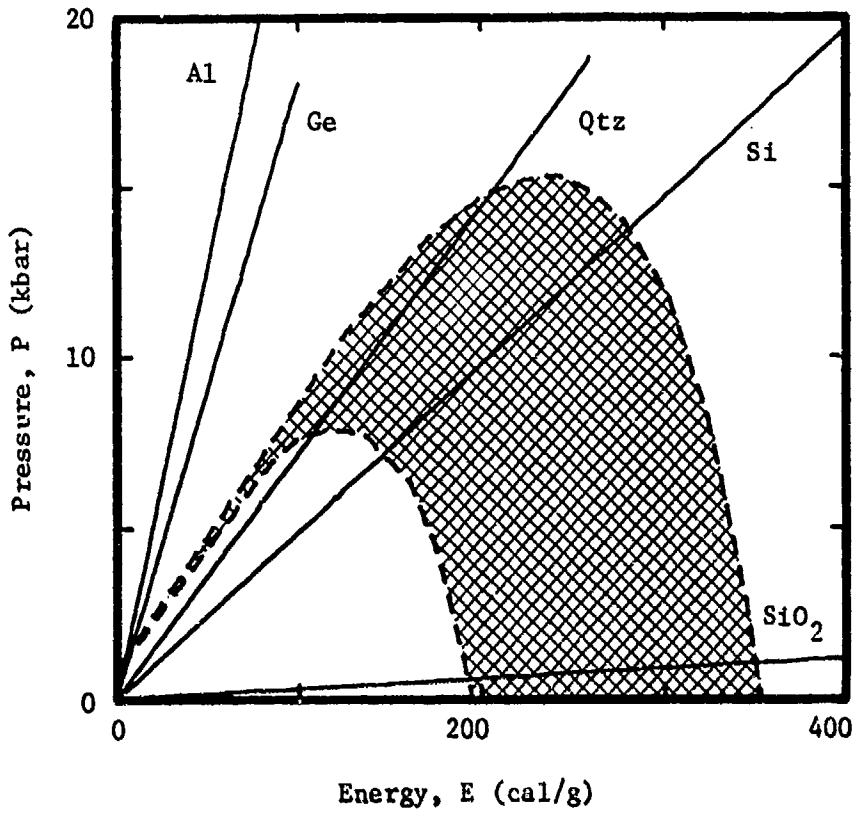

Figure 4. Nominal Pressure-Energy Characteristics for Selected Reference Materials and the Anticipated Sample Characteristics

history (stress profile). The electron beam depth-dose profile and the deposition time both control these requirements.

A simple computer routine was used to predict the energy, stress, and particle velocity profiles from several electron-beam machines for the various reference materials. The inputs required are:

1. depth-dose profile
2. deposition time
3. sample and reference material density, wave speed, Gruneisen parameter, and thickness

Figures 5 and 6 are examples of the predicted stress profiles which exist in the sample and reference material just after deposition. Figure 5 indicates the dependence on mean electron energy (deposition profile). The 8 MeV Hermes beam provides the required regions of uniform pressure while the lower 4 MeV FX-75 beam results in a triangular stress wave, the amplitude of which depends on the time dependent (rather than time integrated) depth-dose profile and on stress-wave attenuation. Figure 6 contrasts the results for the Hermes II and the Aurora beams, both nominally 8 MeV beams with 70 and 140 ns (FWHM) deposition times, respectively. These examples used the following representative sample properties: density - 14 g/cm^3, wave speed - 0.5 cm/μs, Gruneisen parameter - 0.3. X-cut quartz was the reference material.

Based upon these types of considerations, the Hermes II accelerator was selected for the Gruneisen experiments.

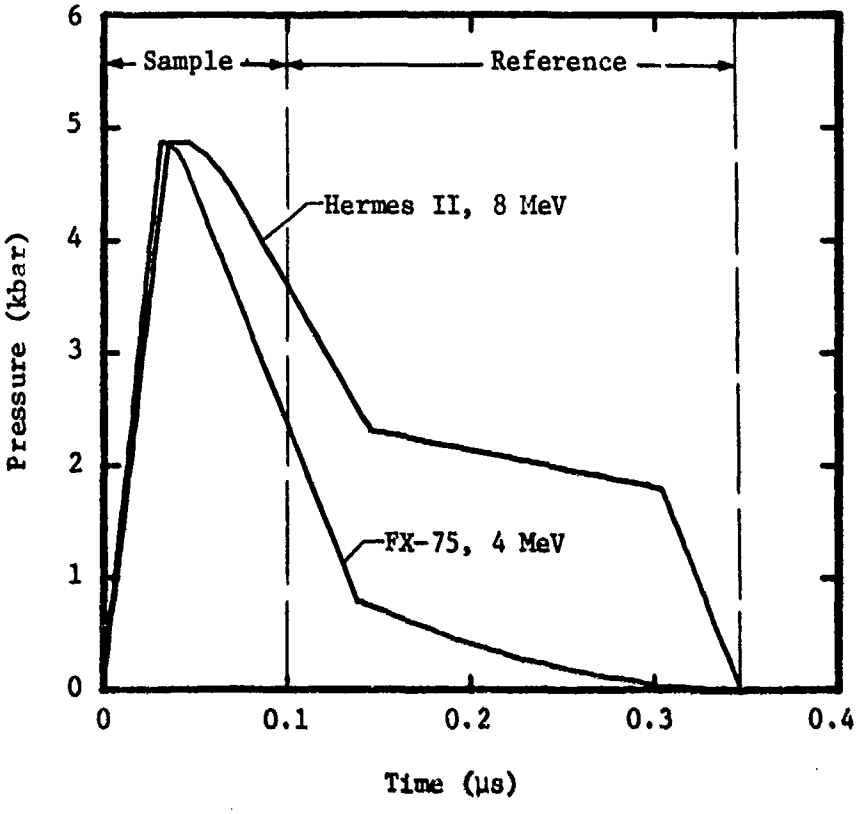

Figure 5. Predicted Response of a Typical Target Configuration Indicating Dependence on Mean Electron Energy

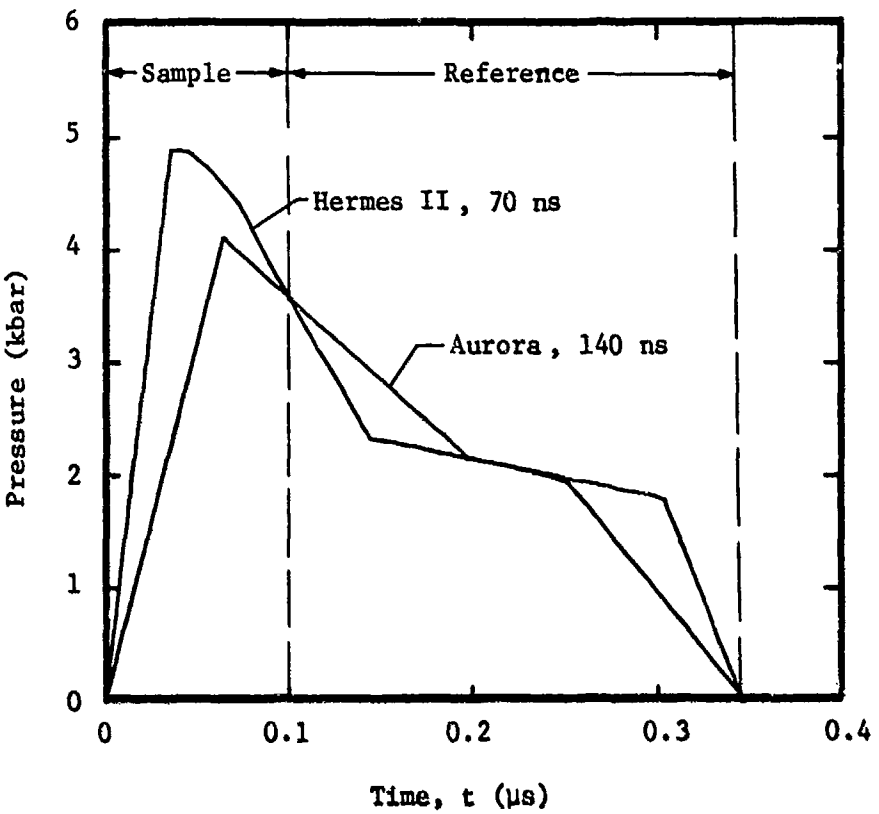

Figure 6. Predicted Response of a Typical Target Configuration Indicating Dependence on Deposition Time

CHAPTER 3
EXPERIMENT CONFIGURATION

This section describes the physical layout of the experiment apparatus, and presents examples of the interferometer data which were recorded for the reference materials.

The target configuration used at the Sandia Laboratories' Hermes II accelerator is shown in Figure 7. Either a sample holding cup or a five-element spatially-resolving graphite calorimeter was positioned in the center of the target assembly. The outer annular area contained twelve calorimeter elements positioned on three radii as shown. The calorimeter thermocouple output voltage was recorded and reduced by the Sandia computer linked data acquisition system (DADS), reference 4. Representative fluence-radius data are presented in Section 4. The velocity of the free rear surface of the reference material was measured with a combination displacement (reference 5) and velocity laser interferometer (reference 6). The velocities in the range below 0.1 mm/μs were best resolved by the displacement interferometer and higher velocities with the velocity interferometer. Greater than normal velocity resolution and the ability to resolve otherwise subtle velocity reversals were obtained with a quadrature system which provides two phase shifted interferometric signals. These signals were transported about 50 feet by a single laser beam from the interferometer to a shielded room where they were optically separated, detected with pulsed photomultipliers, and recorded oscillographically. A second laser beam transported the displacement interferometer signal to the shielded room. This overall setup in the Hermes II facility is shown in Figure 8. The oscillograph and the resultant velocity-time history shown in Figure 9 are representative of the velocity interferometer data. The points in the Figure correspond to the location of the intensity maxima and minima for one quadrature signal. The velocity increment between adjacent intensity extrema is a constant given by (reference 6)

$$\Delta V = \frac{\lambda c}{4L} \qquad (2)$$

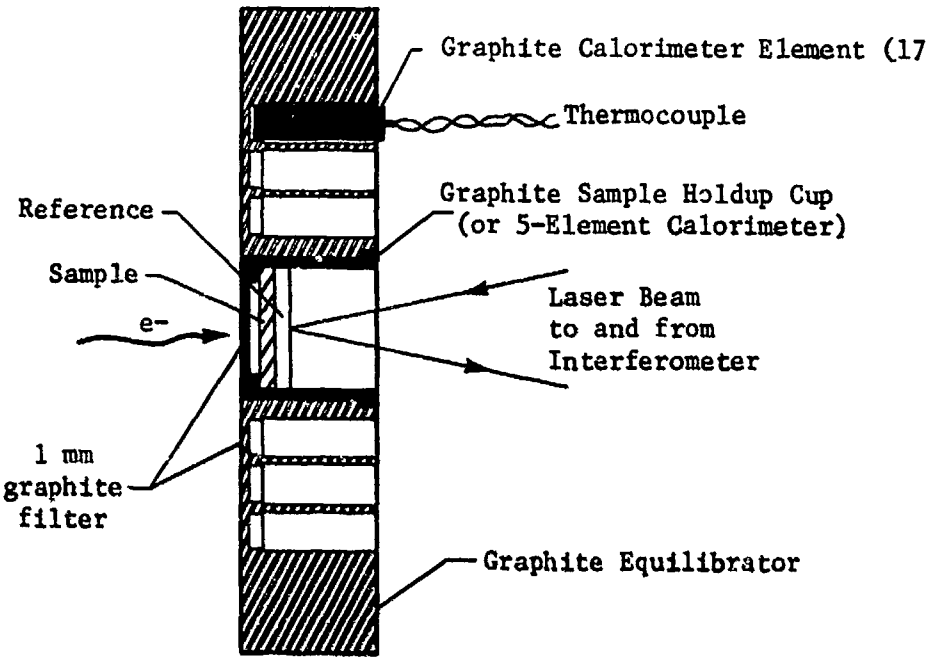

Figure 7. Target and Calorimeter Configuration

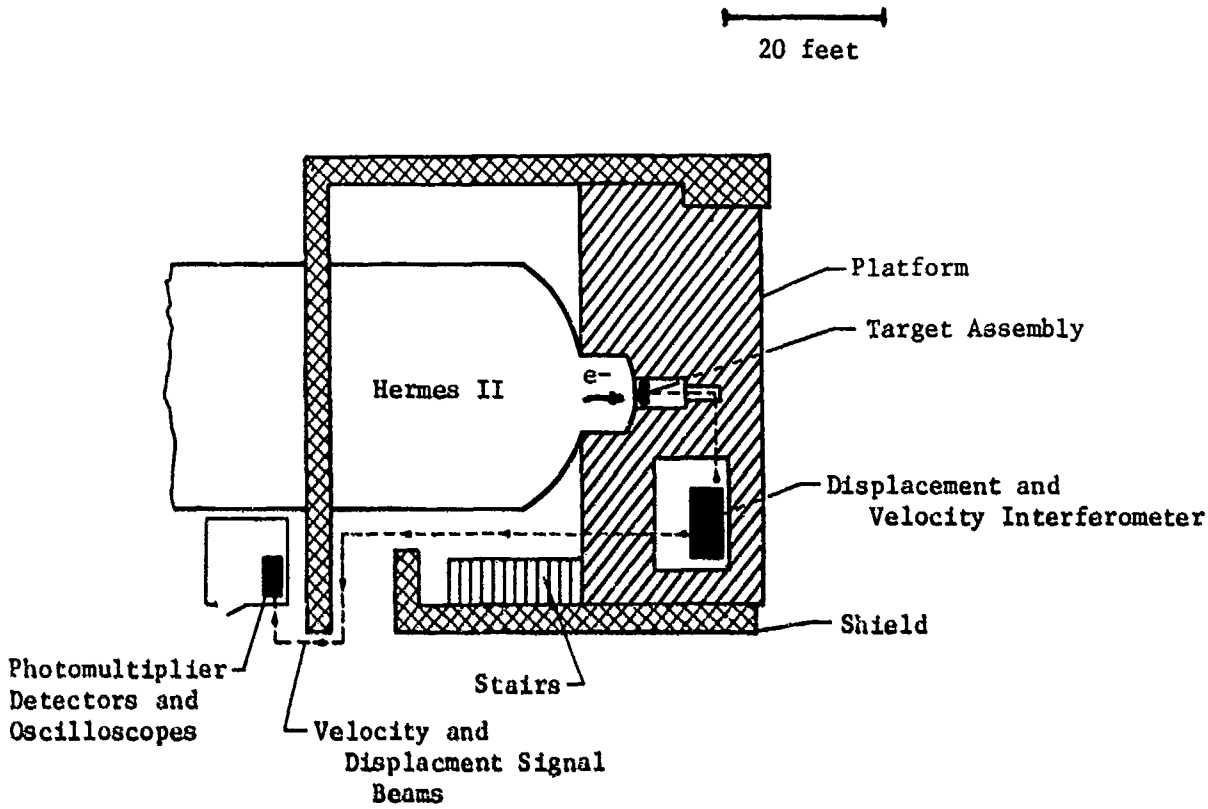

Figure 8. Set Up at the Hermes II Electron Beam Accelerator

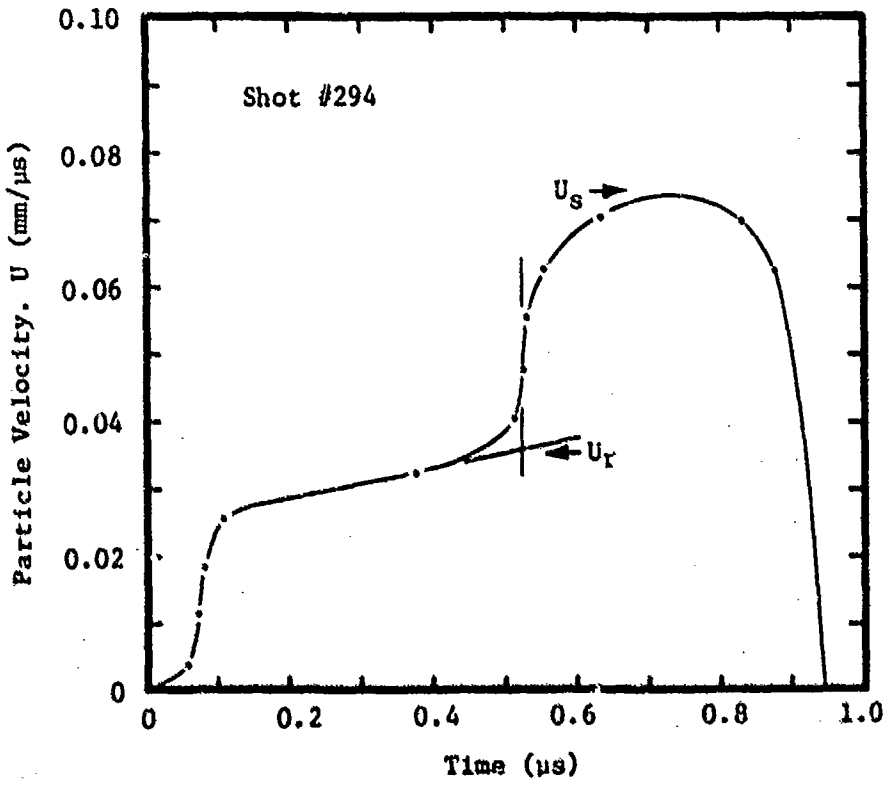

Figure 9. Representative Velocity Interferometer Data for Ge/Qtz Configuration - Shot 294.

where λ and c are the wavelength and speed of light and L is the length of an optical delay path. The velocity-time relation between maxima and minima was obtained from the analytic relation between velocity and intensity (reference 7).

$$U(t) = \frac{\lambda c}{4\pi L} \left\{ \cos^{-1}[2I(t) - 1] \right\} \tag{3}$$

The velocity data shown in Figures 10 and 11 were obtained by differentiating the displacement interferometer data. The points in the figure represent the average velocity over the time interval between N adjacent intensity extrema, which corresponds to a displacement of

$$\Delta x = N\lambda/4 \tag{4}$$

The velocity is, therefore,

$$U = \frac{\Delta x}{\Delta t} = \frac{N\lambda}{4t\Delta t} \tag{5}$$

In the three above representative examples the velocity begins to increase as the beam begins to deposit energy, and the reference plateau is reached about 100 ns later when deposition is nearly complete. The second step is the result of the arrival of the stress wave from the sample.

The characteristic "reference" and "sample" material particle velocities (U_r and U_s) are indicated on the figures. These velocities are selected and used in the analysis procedure as described in Section 5 to determine the intermediate adiabatic expansion stress state, which is close to the Gruneisen stress, and thence the Gruneisen stress state of interest.

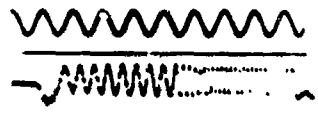

0.1 μs/Time Mark

Base Line

Interferometer Signal

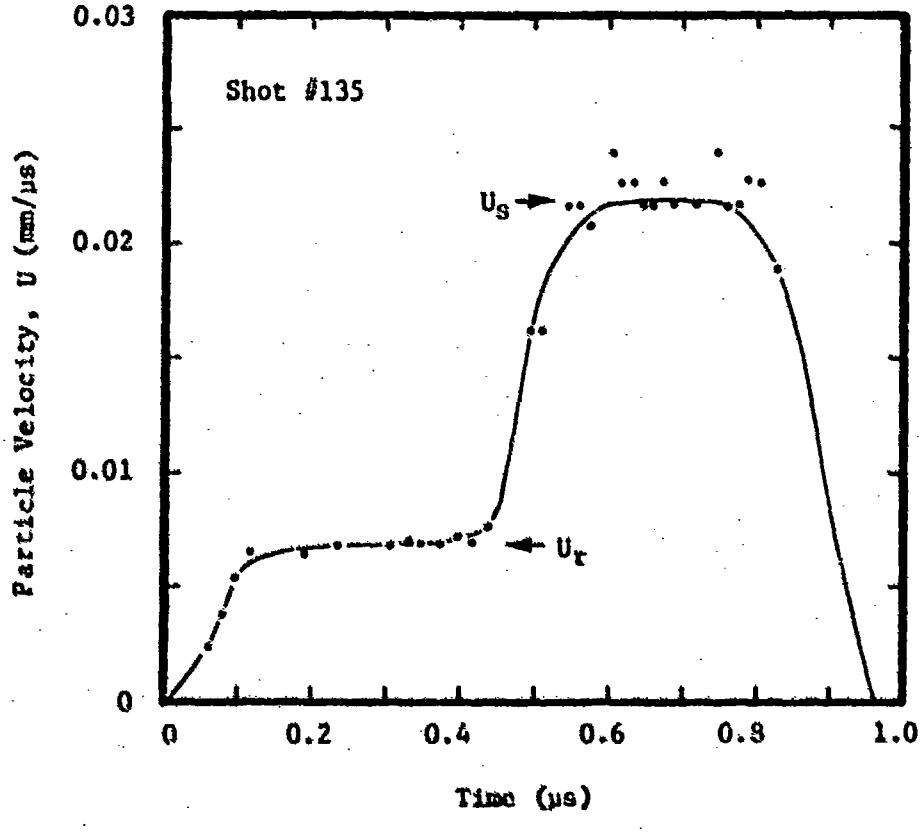

Figure 10. Representative Displacement Interferometer Data for Qtz/Si Configuration - Shot 135

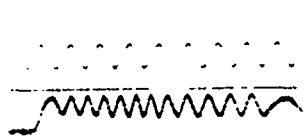

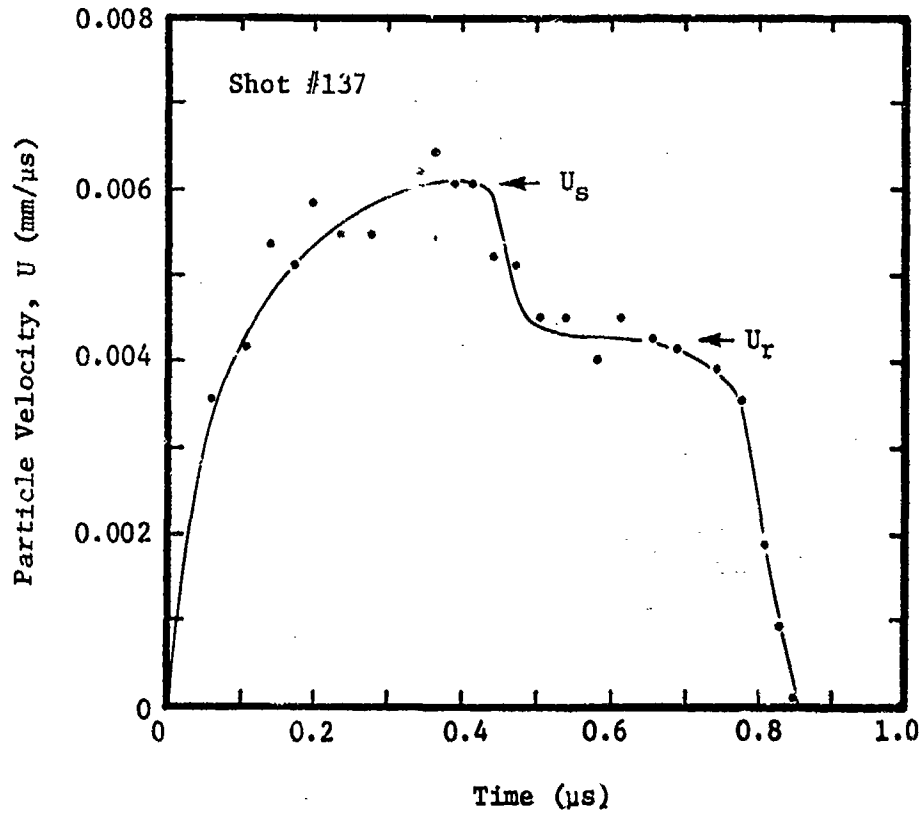

Figure 11. Representative Displacement Interferometer Data for Si/Qtz Configuration - Shot 137

CHAPTER 4

ELECTRON BEAM CHARACTERIZATION

The Hermes II pulsed electron-beam machine was used as the electron source for all the experiments described in this report. The machine and facilities are described in detail in reference 8 and the general performance data are given in Table 1. Diode current and voltage data were taken for each of about 100 shots conducted under this program.

The depth-dose profile was determined from the thermoelastic response of a 0.50-inch thick X-cut quartz crystal. The rear free surface particle velocity time history was measured with a laser velocity interferometer. Transport calculations were made with the ELTRAN (reference 9) Monte Carlo code using the electron energy spectrum determined from the diode current and voltage diagnostic data for the shot and various incident angles. The measured and computed depth-dose relations are normalized to the absorbed energy and compared in Figure 12. The best fit to the experimental data was obtained for an assumed incidence angle of 30 degrees. This angle was used for all other calculations presented in this report.

Calculations were made with several representative spectra determined from diode data representing the range of mean electron energies obtained throughout the tests, and the peak dose (energy coupling coefficient) was observed to vary by ± 5 percent.

The spectrum shown in Figure 13 for shot No. 139 was chosen as producing the most representative depth-dose profile and all calculations utilize this spectrum. Also, all other calculations are normalized to incident fluence and all fluence data are corrected to incident fluence as described below. Figure 14 presents the ELTRAN results for this spectrum incident at 30 degrees to carbon (atomic number, Z = 6), germanium (Z = 32) and tantalum (Z = 73). Calculations for actual bi-laminate target configurations are presented in Sections 6 for the reference material experiments and in Part II for the porous sample configurations. The

TABLE 1

HERMES II ACCELERATOR GENERAL CHARACTERISTICS

Marx Generator Voltage	70.0 kV
Peak Diode Voltage	9.4 MV
Peak Diode Current	11.5 kA
Mean Electron Energy	7.8 MeV
Pulse Width (FWHM, power)	70 ns
Total Beam Energy	76 kj

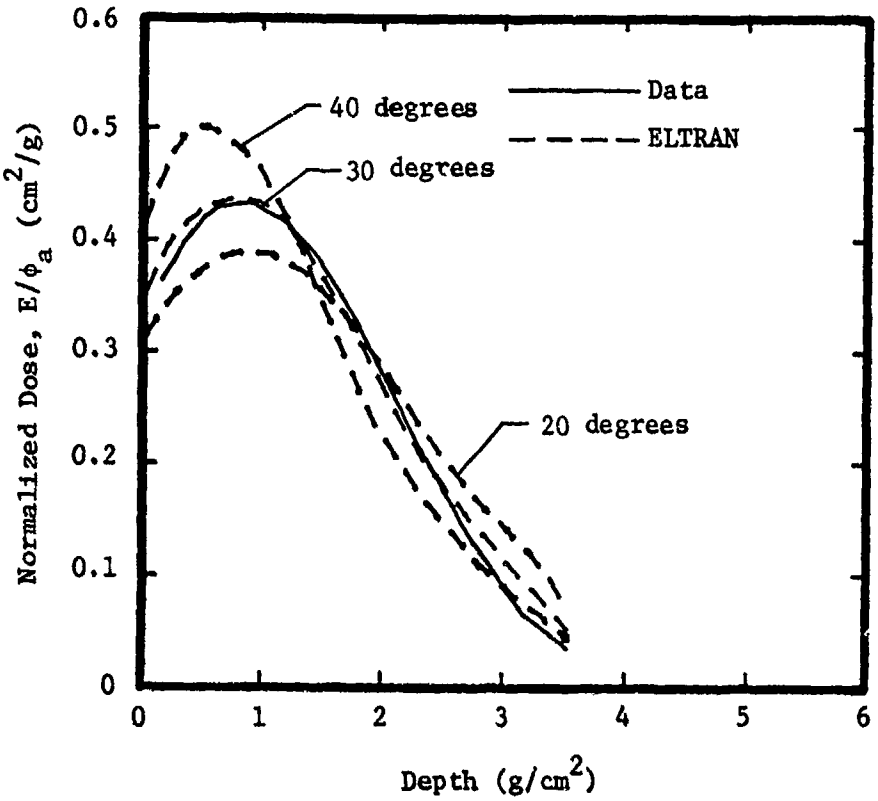

Figure 12. Measured and Computed Depth-Dose Relations for Quartz

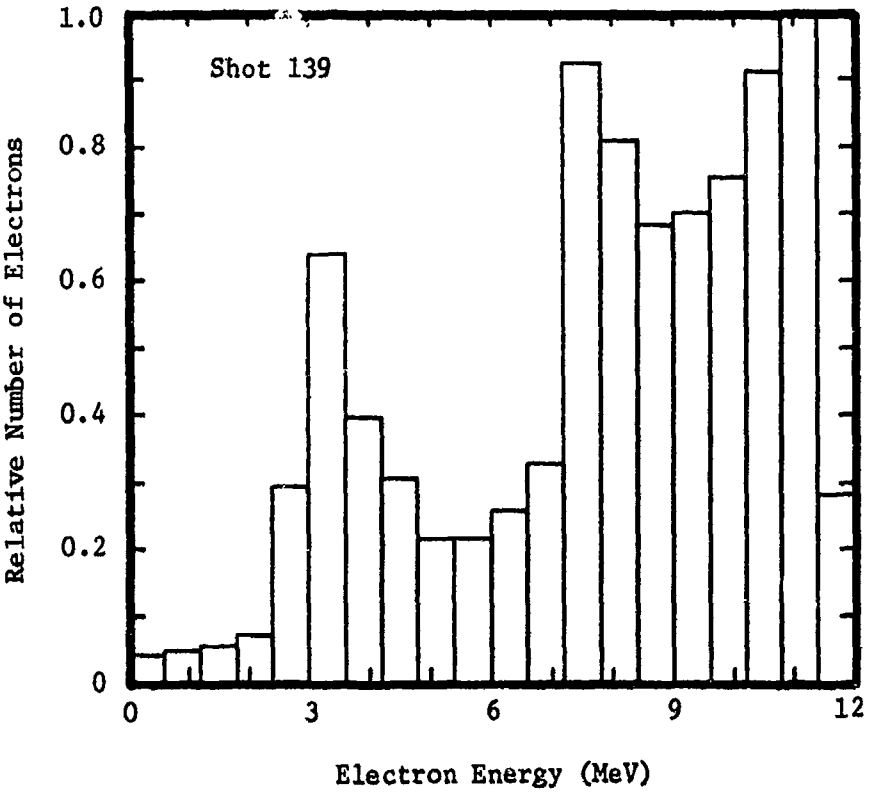

Figure 13. Electron Spectrum

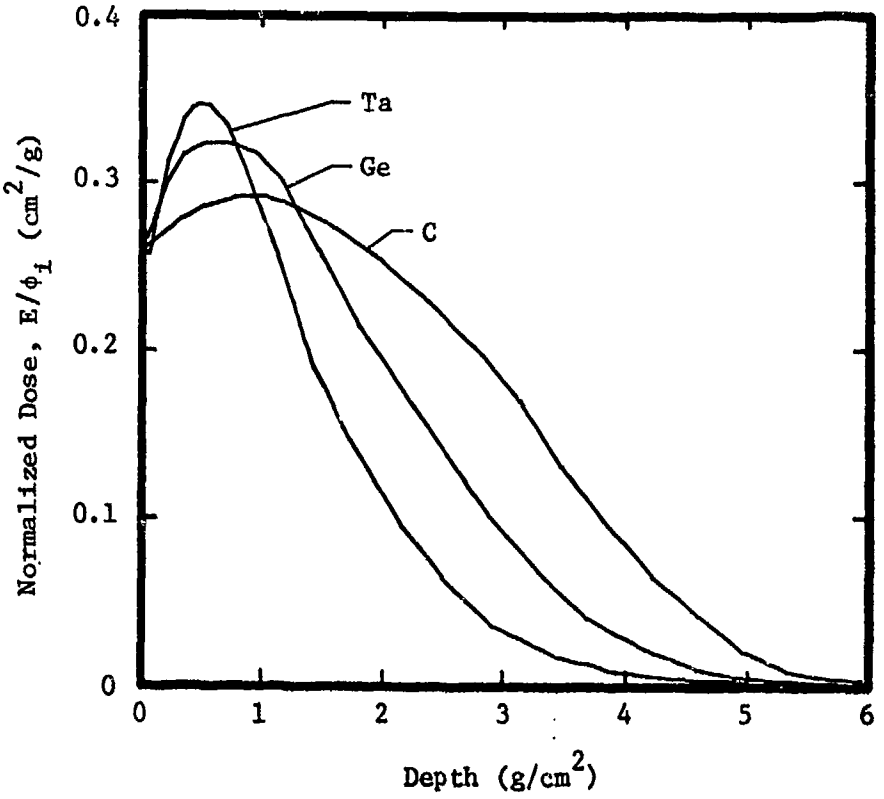

Figure 14. Depth-Dose Calculations for Three Materials

deposition profile was flat to within 5 percent across the sample, with the aid of a thin 0.176 g/cm^2 carbon filter.

The deposited energy-versus-time characteristics as determined from diode data are shown in Figure 15. The 70 ns linear approximation shown is the full width at half maximum of the power curve, and is suggested for use in time-dependent material response calculations.

Fluence data were taken with a spatially resolving graphite calorimeter (shown previously in Figure 7). The center five elements were interchangeable with the sample holding cup so that peripheral fluence measurements could be made during sample shots. All the absorbed fluence data reported here are converted to incident fluence based on electron deposition calculations for graphite which show that a total of 12.4 percent of the incident energy is lost by absorption in the 0.1 cm thick filter, by Bremsstrahlung and by backscattering. Three representative sets of fluence-radius data are given in Figure 16 for shots with peak fluences of 300, 150, and 50 cal/cm^2.

The various fluence levels were obtained by adjusting the axial distance from the anode to the target/calorimeter assembly. The highest fluence, about 300 cal/cm^2, was obtained at the "first pinch", which occurs at about 13 cm from the anode plane. This is less than half of the peak fluence anticipated based on data presented in reference 10, which were taken with a larger diameter drift tube (71 cm versus our 18 cm tube), and this may have resulted in a more intense pinch. Thus, the peak dose in our experiments was about 100 cal/g.

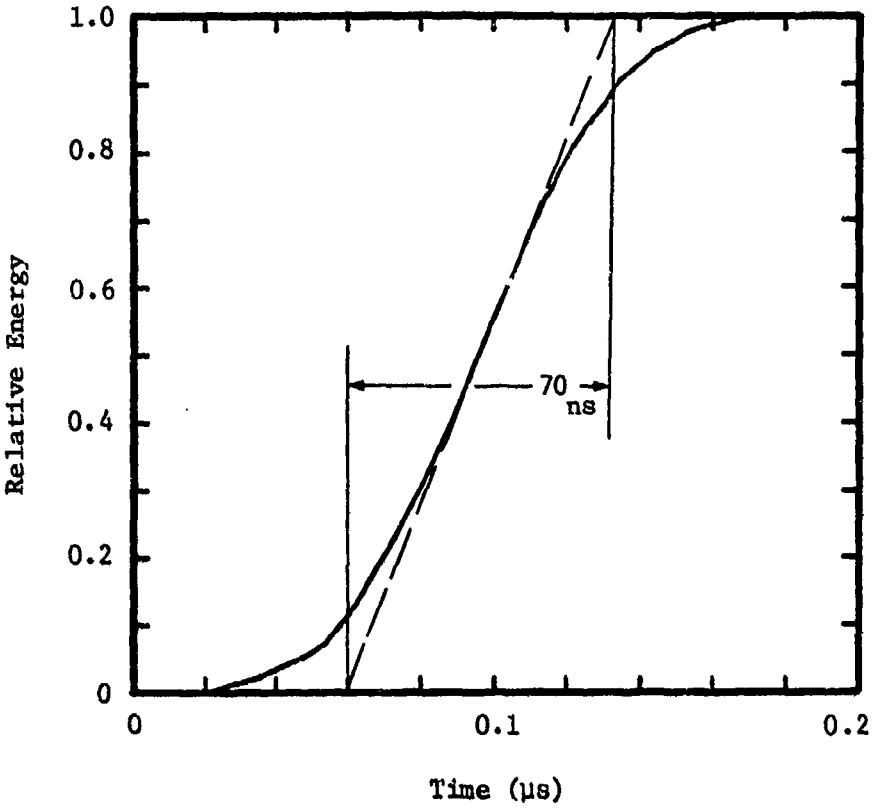

Figure 15. Deposited Energy Time Characteristics. (70 ns is the FWHM of the power curve)

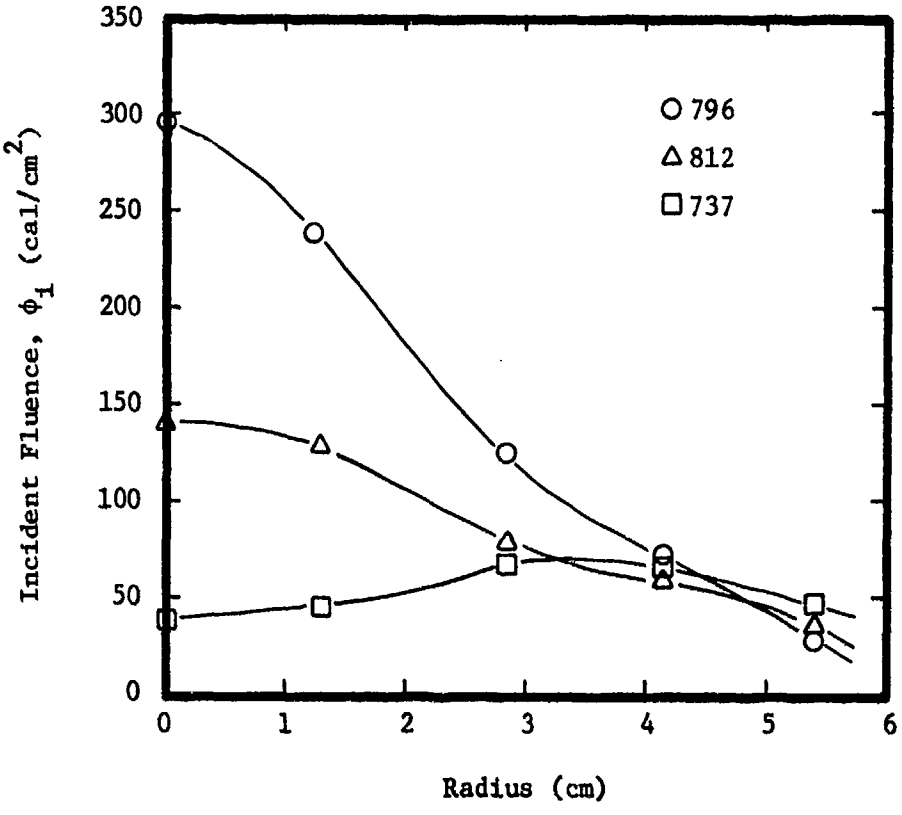

Figure 16. Representative Fluence-Radius Data

CHAPTER 5
ANALYSIS PROCEDURES

This Section describes the procedures used to compute the initial sample pressure-energy state and other related parameters of interest.

The rear free surface velocites U_r and U_s are defined by the amplitude of the first and second velocity steps respectively. Since the deposition is not instantaneous and uniform through the thickness of the sample and reference materials, the step amlitudes are determined as indicated in Figures 9, 10, and 11. The maximum velocity occurring near the center of the "sample step" is taken as U_s. The velocity found by extrapolating the reference step to the sample-reference interface is taken as U_r.

Figure 17 indicates the adiabatic paths which relate the measured step amplitudes U_r and U_s to the initial (Gruneisen) pressures P_r and P_s. The sample adiabat is represented by a solid line and the reference material adiabats by dashed lines. All reference material adiabats are assumed to be linear for purposes of this discussion. The sample adiabat is assumed to be linear between P_a and P_s. Note the existence of intermediate states which are defined by the Hugoniot continuity and conservation requirements. The intermediate state on the sample adiabat (U_a, P_a) can be found from the measured velocities U_r and U_s and the known reference material adiabats. For the case of linear reference material adiabats with constant slope Z_r the relations are simply

$$P_a = 1/2\ Z_r(U_r + U_s) \tag{6}$$

and

$$U_a = 1/2\ (U_s - U_r) \tag{7}$$

These relations define a point on the sample adiabat centered at the initial heated state. Note that various points on the sample adiabat from

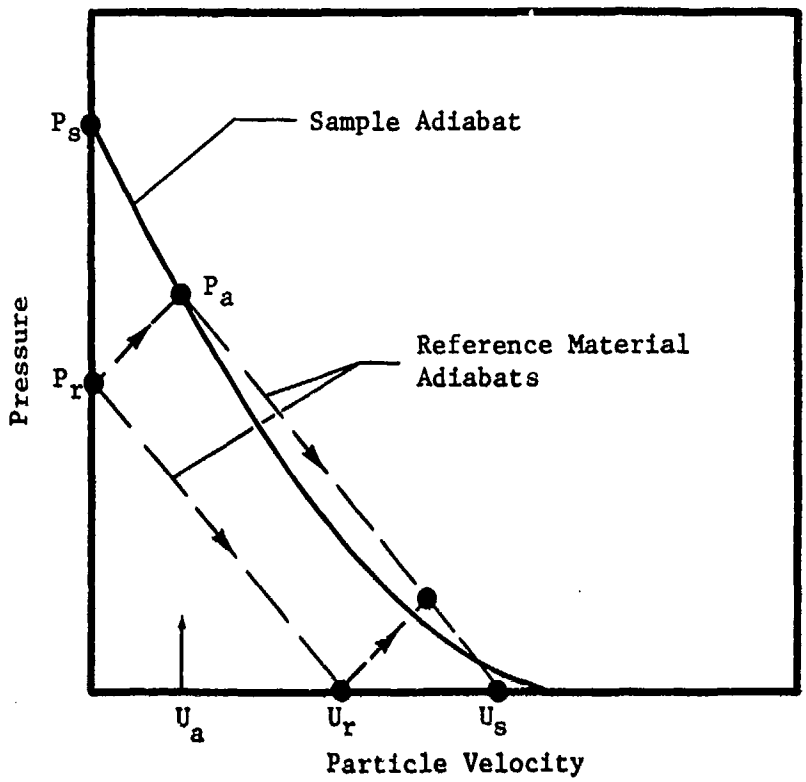

Figure 17. Adiabatic Paths Relating Measured and Calculated States

the same initial P_s, E_s state may be determined by repeating the experiment with different reference materials which generate different initial pressures P_r's, and have different adiabat slopes. If the initial reference material pressure is greater than the initial sample material pressure ($P_r > P_s$), a point on the sample's compression curve is determined. In this case the reference material is placed in tension, which may result in fracture (spall) of the reference material, precluding the measurement of U_s at the reference rear surface. Figure 11 is an example of such a case which did not result in spallation. If the initial reference material pressure is less than the initial sample material pressure ($P_r < P_s$), a point on the expansion adiabat is determined. By using different reference materials, a complete adiabat can be mapped from the initial P_s, E_s state.

If the sample adiabat shape between P_a and P_s is known, the initial sample pressure P_s can also be obtained from U_s and U_r. If the portion of the sample adiabat connecting the initial state with the intermediate state is assumed to be linear with slope Z_s in the P - U plane, the initial sample (Gruneisen) pressure is:

$$P_s = P_r + 1/2(Z_r + Z_s)(U_s - U_r) \tag{8}$$

where

$$P_r = Z_r U_r \tag{9}$$

For linear elastic sample and reference materials, the adiabat slopes are simply

$$Z_s = \rho_s D_s \tag{10}$$

and

$$Z_r = \rho_r D_r \tag{11}$$

where ρ and D are the initial density and the dilatational wave velocity

in the direction of wave propagation. In order to simplify data analysis, it is highly desirable to utilize linear elastic reference materials.

For porous or composite sample materials the adiabat slopes are not constant and the local wave speed can vary more than a factor of two between the initial P_s,E_s state and the expanded zero pressure state. In general, the slope along the adiabat is given by

$$Z_s(P) = \frac{\partial P}{\partial V} = \rho_s D(P) \tag{12}$$

where D(P) is the local Lagrangian wave speed. E-beam wave transit time data were used to obtain an effective adiabat slope Z_s for the segment between P_a and P_s as follows.

After deposition, relief waves propagate toward each other from the sample material surfaces meeting in the center. The velocity of the leading edge of these waves is $D(P_s)$. From the center of the sample a wave then propagates to the elastic reference material at velocity $D(P_a)$. The average wave speed found by measurement of the sample-step pulse-width is therefore (neglecting the very small particle velocities):

$$D_s \approx \frac{x}{t} = \frac{D(P_s) + D(P_a)}{2} \tag{13}$$

where x is the sample thickness. Therefore, D_s computed as x/t may be used to obtain an effective adiabat slope for use in the linear analysis scheme, Equation (8). The experimental relief wave speeds agreed with the literature values (see Chapter 6, Table 3).

As the pressure generated in the reference material P_r approaches the sample pressure P_s the portion of the sample adiabat joining the desired P_s,E_s state with the point on the sample adiabat becomes shorter and, therefore, the uncertainty in the measurement of P_s decreases (dependence on $Z_s = \rho D_s$ is relaxed.) It is therefore desirable to use a reference material which closely matches the pressure generated by the sample.

The change in internal energy E_r for a particular test can be directly determined from the initial reference material response since

$$E_r = \frac{P_r}{\gamma_r \rho_r} \tag{14}$$

and P_r is known by Equation (9). If the sample and reference materials achieve slightly different energy states because of non-uniform deposition, the sample energy state is determined from the coupling coefficient ratio

$$E_s = \frac{C_s}{C_r}(E_r) \tag{15}$$

The coupling coefficeints are defined as follows:

$$C_s = E_s/\phi_i \tag{16}$$

and

$$C_r = E_r/\phi_i \tag{17}$$

where ϕ_i is the incident fluence. The appropriate coupling coefficients are found from ELTRAN calculations (Section 4) and are selected to correspond to the measured particle velocities U_r and U_s, as described in Section 3; i.e., C_s is the peak value and C_r is the value at the sample-reference interface. (The values for the reference material test configurations are given in Section 6, Table 2.)

CHAPTER 6

RESULTS FOR REFERENCE MATERIALS

In order to exercise the stress-matching technique on porous and composite materials of interest, the thermomechanical response of a group of appropriate reference materials was verified. Several candidate reference materials were chosen based on the anticipated pressure-energy response of the porous sample materials, the response of which is discussed in Part II. These reference materials were evaluated (calibrated) by performing thermomechanical response measurements in the previously described test configuration in which two candidate reference materials were exposed in each test. One material in the "sample" position (nearest to the pulsed electron source) and the other in the "reference" position. The rear free surface particle velocity of the reference material was measured to provide the step particle velocity amplitudes U_r and U_s as described previously.

The energy coupling coefficients were determined from ETRAN code Monte Carlo deposition calculations based on beam characteristics established in Section 4. Deposition calculations were made for each test configuration. Representative deposition profiles are given and compared with the nominal carbon deposition profile in Figures 18 to 20. Table 2 summarizes the deposition profile data in terms of the energy coupling coefficients C_r and C_s for each test configuration.

Based on the analysis scheme described in Section 5, the various pressure, energy, and particle velocity states were computed from the coupling coefficients and measured free surface particle velocities. The reference material parameters which were used in the data analysis are given in Table 3.

The measured and computed data for the reference materials are summarized in Table 4, and the pressure-energy data are plotted in Figure 21. The Gruneisen parameters were obtained from the slope of

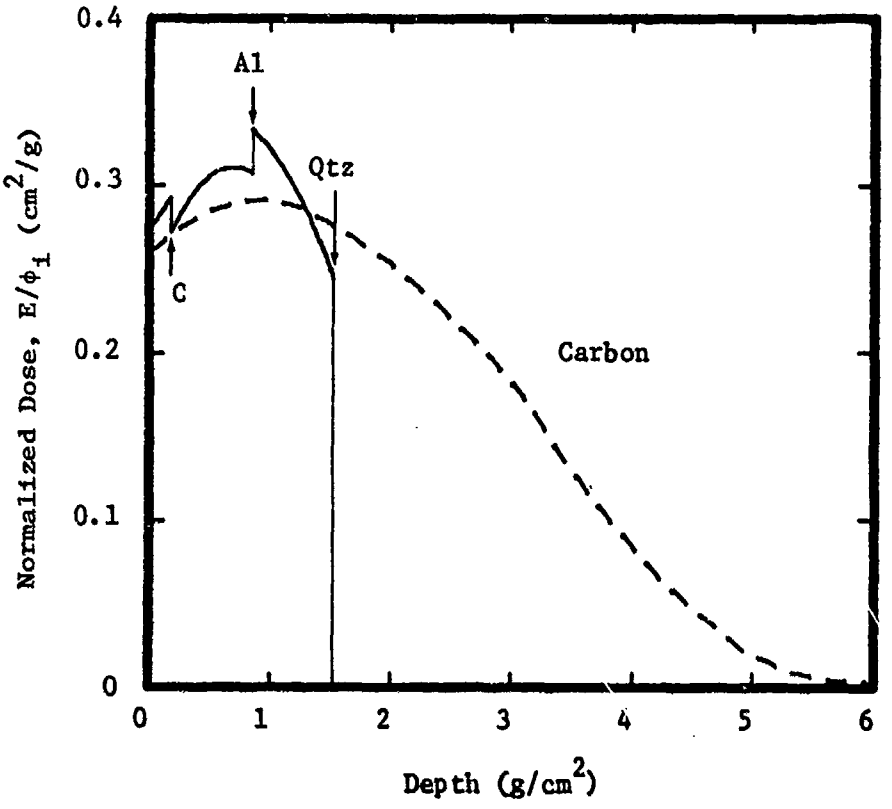

Figure 18. Deposition Profile for Al/Qtz Configuration

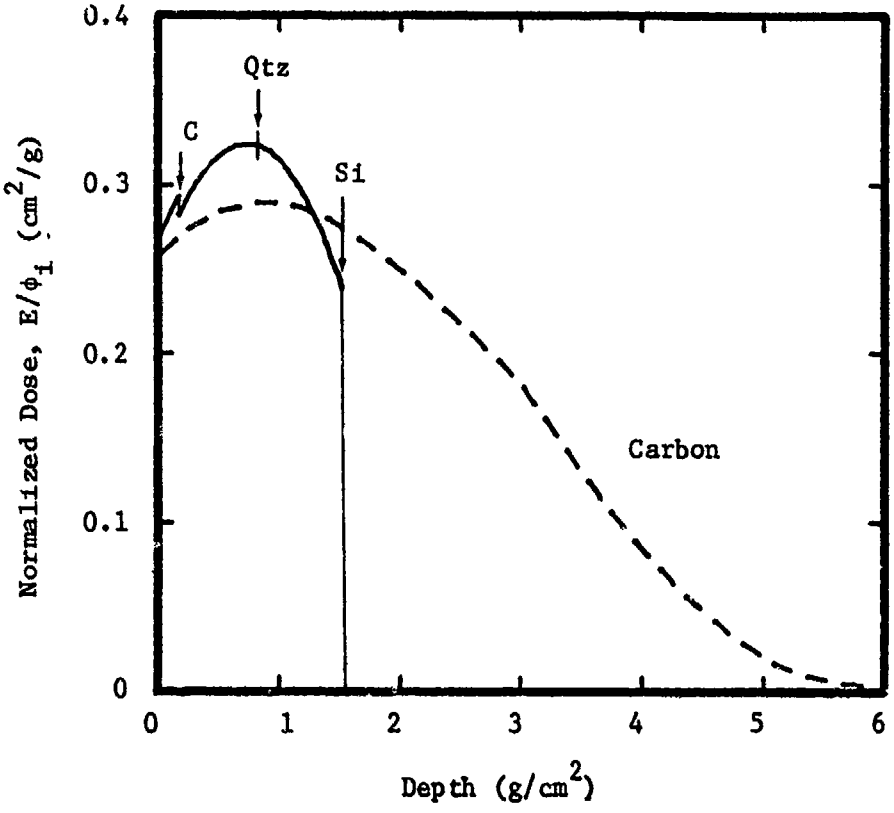

Figure 19. Deposition Profile for Qtz/Si Configuration

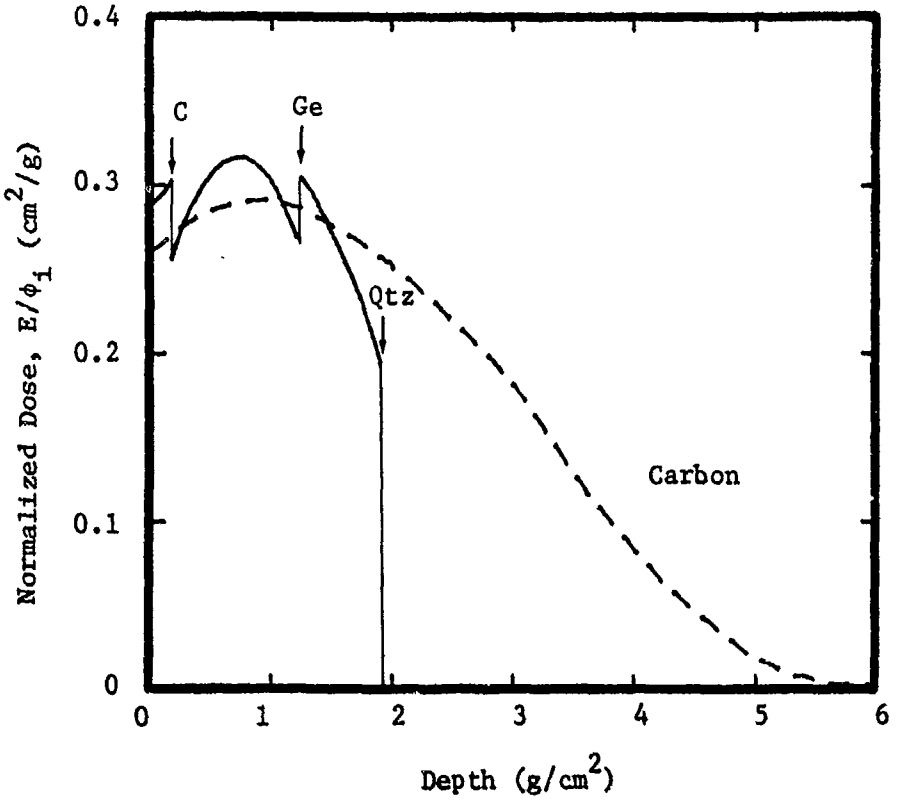

Figure 20. Deposition Profile for Ge/Qtz Configuration

TABLE 2

ENERGY COUPLING COEFFICIENTS

FOR THE REFERENCE MATERIAL TEST CONFIGURATIONS

Configuration		Energy Coupling Coefficients (cal/g)/(cal/cm^2)		Thickness (cm)	
Sample	Reference	Sample C_s	Reference C_r	Sample	Reference
Al	Qtz	0.31	0.33	0.25	0.26
Ge	Qtz	0.32	0.31	0.20	0.26
Si	Qtz	0.34	0.33	0.30	0.26
Qtz	Si	0.34	0.33	0.26	0.30
Ge	Si	0.32	0.31	0.20	0.30

TABLE 3

REFERENCE MATERIAL PARAMETERS USED IN THE DATA ANALYSIS

Material	Density (g/cm^3)	Wave Speed ($cm/\mu s$)
Aluminum (6061-T6)	2.70	0.64
Quartz (X-cut)	2.65	0.572
Germanium (111)	5.32	0.550
Silicon (polycrystal)	2.33	0.593

TABLE 4. REFERENCE MATERIAL DATA SUMMARY

Shot No.	Test Configuration (Sample/Reference)	Reference Material: Measured Particle Velocity U_r (mm/μs)	Reference Material: Dose E_r (cal/g)	Reference Material: Pressure P_r (kbar)	Reference Material: Gruneisen Parameter γ_r	Sample Material: Measured Particle Velocity U_s (mm/μs)	Sample Material: Dose E_s (cal/g)	Sample Material: Pressure P_s (kbar)	Sample Material: Gruneisen Parameter γ_s
133	Al/Q	0.006	12.6	0.91	0.65	0.018	11.8	2.86	2.13
135	Al/Q	0.007	14.7	1.06	0.65	0.022	13.8	3.50	2.23
293	Al/Q	0.0480	101	7.28	0.65	0.1398	94	22.2	2.06
138	Ge/Q	0.0045	9.43	0.68	0.65	0.0105	9.7	2.01	0.93
294	Ge/Q	0.0380	80	0.68	0.65	0.0760	82	14.2	0.77
751	Ge/Q	0.0280	59	4.24	0.65	0.0580	61	10.91	0.81
137	Si/Q	0.006	12.6	0.91	0.65	0.0042	12.1	0.58	0.48
141	Si/Q	0.0315	66.00	4.77	0.65	0.0250	66	3.6	0.56
136	Q/Si	0.0025	10.7	0.52	0.50	0.004	10.7	0.80	0.67
286	Q/Si	0.0240	103	0.52	0.50	0.0340	103	6.84	0.60
308	Q/Si	0.0170	73	3.56	0.50	0.0310	73	6.09	0.75
753	Q/Si	0.0135	58	2.83	0.50	0.0250	58	4.10	0.64
287	Ge/Si	0.0300	103	5.0	0.50	0.0560	106	19.1	0.81

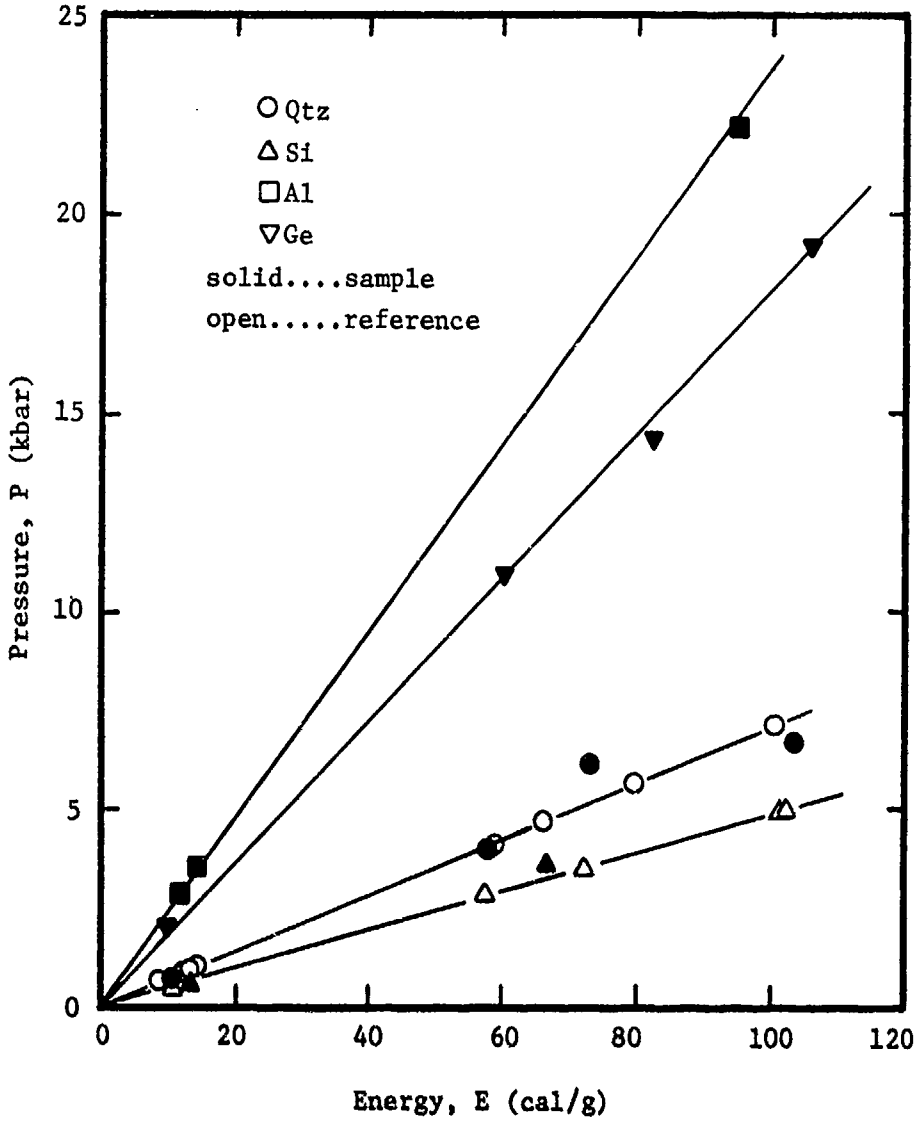

Figure 21. Pressure-Energy Data for Reference Materials

least-squares straight line fits to the pressure-energy data shown in Figure 21; they are normalized to be consistant with the value $\gamma = 2.1$ for aluminum, which is used in determining the deposited energies. The resulting Gruneisen parameters are given in Table 5 and are compared with calculated (thermodynamic) values and with results previously measured at low dose (< 10 cal/g).

An alternate approach with which the Gruneisen parameters were computed from incident fluence determined "statistically" from the fluence measurements which were interspersed with data shots provided less consistent results. This result is attributed to: (1) lack of machine repeatability, and (2) inaccuracies in the fluence measurement process. Extrapolating the peripheral fluence calorimeter data to obtain fluence at the central sample location also provided inconsistent results. These results are exemplified by the fluence data for a series of shots presented in Figure 22. This figure presents the axial fluence as determined by (1) direct measurement by carbon fluence calorimeter, (2) by extrapolation of peripheral fluence calorimeters, and (3) by computation from the reference material response and the Gruneisen parameters of this work given in Table 5. All measured (absorbed) fluence data are corrected to incident fluence as described in Section 4. These fluence results emphasize the importance of obtaining a direct fluence measurement via the reference material response, on each specimen test.

TABLE 5

MEASURED AND REFERENCED GRUNEISEN PARAMTERS

Material	γ From This Work[a]	γ Calculated from Thermodynamic Data[b]	γ From Other E-Beam Measurements[c]
Aluminum	2.10	2.17[n] 2.14 - 2.19[d]	2.11[f] 2.07[g]
Quartz	0.65	0.74[e]	0.67[h] 0.65[i]
Germanium [111]	0.76	0.72[l] 0.80[d]	0.75[g]
Silicon* (polycrystal)	0.50	0.57[d] 0.43[m]	0.46[j] 0.42[k]

[a] Relative to $\gamma_{Al} = 2.10$

[b] $\gamma = \beta/\rho K C_p$

[c] All measurements at relatively low dose, < 10 cal/g

[d] Reference 11

[e] Reference 3

[f] Reference 12

[g] Reference 13

[h] Relative to $\gamma_{Al} = 2.10$, Reference 3

[i] Reference 14

[j] Relative to $\gamma_{Al} = 2.10$, Reference 3, [111] Si*

[k] Reference 13, [111] Si*

[l] Reference 15

[m] [111] Si*, Reference 15

[n] Reference 16

* For crystals of cubic symmetry such as Si and Ge, the same γ is obtained for a single crystal and a polycrystal.

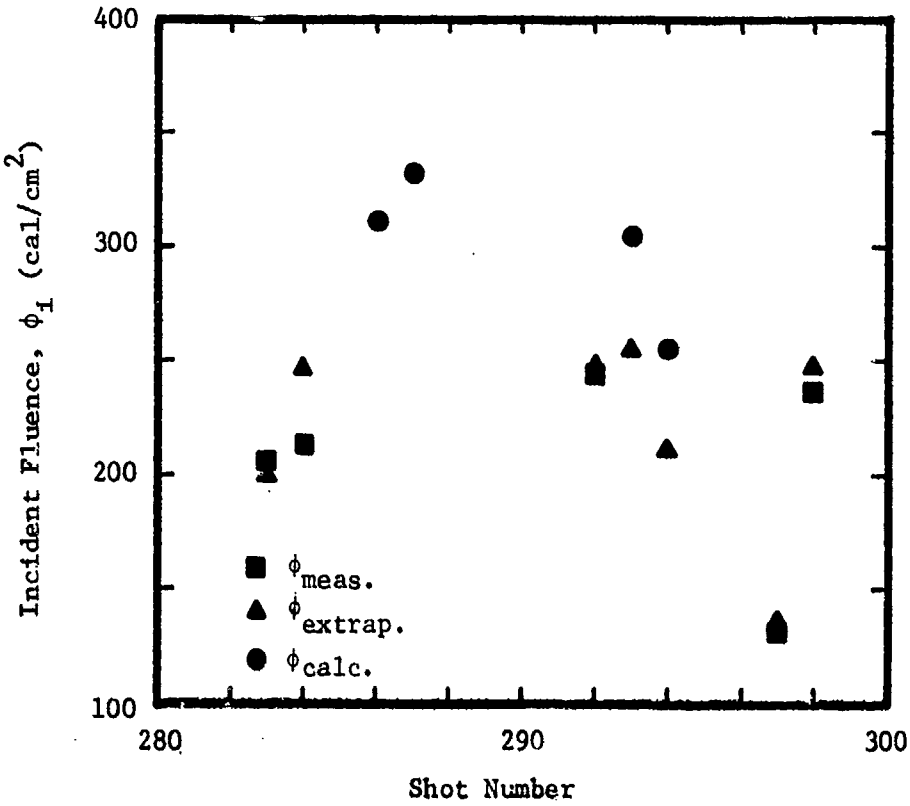

Figure 22. Fluence Data as Measured, Extrapolated and Computed from Reference Material Response

CHAPTER 7
CONCLUSIONS

1. The pressure-energy relations have been measured to 100 cal/g for four reference materials (Al, Qtz, Si, Ge). Data at greater doses would be of value in extending the range of usefulness of these reference materials.

2. The four reference materials can be treated as linear and elastic in this range of thermomechanical response. Measured Gruneisen values agreed to ± 10 percent with calculated values using thermodynamic properties. The following Gruneisen parameters were established:

Aluminum (6061-T6), $\gamma = 2.10$

Germanium [111], $\gamma = 0.65$

Quartz (X-cut), $\gamma = 0.76$

Silicon (polycrystal), $\gamma = 0.50$

3. The concept of using the reference material to provide an in-situ measurement of dose (fluence) was proven, and it was shown to be necessary because of machine non-repeatability.

4. The concept of using pressure generating reference materials to provide more accurate measurement of initial sample stress without heavy dependence on the sample adiabat was demonstrated. Part II of this report describes the application of this concept to determine the Gruneisen parameters of porous metals and cermets.

CHAPTER 8

REFERENCES

1. Oswald, R. B., Jr., Mclean, F. B., Schallhorn, D. R., and Oldham, T. R., "Dynamic Response of Aluminum to Pulsed Energy Deposition in The Melt-Dominated Regime," J. Appl. Phys., 44, No. 8, pp. 3563-3374, (1973).

2. Perry, F. C., J. Appl. Phys., 41, p. 4208 (1970).

3. Graham, R. A., and Hutchinson, R. E., "Thermoelastic Stress Pulse Resulting from Pulsed Electron Beams," Appl. Phys. Letters, 11, No. 2, (15 July 1967).

4. Bailey, F. A., Operation of the DADS System for Hermes II, REBA Calorimetery, SC-TM-70-821, Sandia Laboratories, Albuquerque, N.M., to be published.

5. Barker, L. M., and Hollenback, R. E., "Interferometer Technique for Measurement of the Dynamic Properties of Materials", Rev. of Sci. Inst., 36, 1617 (1965).

6. Barker, L. M., and Hollenback, R. E., "Shock-Wave Studies of PMMA, Fused Silica, and Sapphire," J. of Appl. Phys., 41, p. 4208 (1970).

7. Froula, N., Bryson, R., and Suenaga, E., A Computer Program for Reducing Laser Velocity Interferometer Data, 3SR-1101, Systems, Science, and Software, La Jolla, California (June 1972).

8. Chodorow, A. M., Hermes II Experimenters' Manual, SC-M-70-242, Sandia Laboratories, Albuquerque, N.M. (June 1970).

9. Brittain, F. H., A Description of ELTRAN: An Electron Deposition Code, SC-TM-68-713, Sandia Laboratories, Albuquerque, N.M. (January 1969).

10. Schulze, J. F., A Method for Making Electron Beam Measurements on Hermes II, SC-TM-72 0649, Sandia Laboratories, Albuquerque, N.M., (March 1973).

11. Gschneidner, A., Jr., "Physical Properties and Interrelationships of Metallic and Semimetallic Elements," Solid State Phys., 16, 275 (1964).

12. Perry, F. C., "Thermoelastic Response of Polycrystalline Metals to Relativistic Electron Beam Absorption," J. Appl. Phys., 41, 5017 (November 1970).

REFERENCES (Continued)

13. Oswald, R. B., Jr., McLean, F. B., Schallhorn, D. R., and Oldham, T. R., "Gruneisen Data from the Free Surface Velocity of Thermoelastic Materials," J. Appl. Phys., 44, 561 (February 1973).

14. Gauster, W. B., Perry, F. C., and Buckalew, W. H., "Pressure Response of a Solid Pulse-Heated through a Polymorphic Phase Transition: The $\alpha - \beta$ Inversion in Quartz," J. Appl. Phys., 44, 4970 (November 1973).

15. Gibbons, D. F., "Thermal Expansion of Some Crystals with the Diamond Structure," Physical Rev., 112, 136 (October 1958).

16. Kittel, C., Introduction to Solid State Physics (John Wiley & Sons, Inc., N.Y.), p. 155, (1961).

DISTRIBUTION LIST

DEPARTMENT OF DEFENSE

Director
Defense Advanced Rsch. Proj. Agency
ATTN: Strategic Tech. Office

Defense Documentation Center
Cameron Station
12 cy ATTN: TC

Director
Defense Intelligence Agency
ATTN: DT-2 Wpns. & Sys. Div.

Director
Defense Nuclear Agency
ATTN: TISI Archives
ATTN: SPSS
ATTN: SPAS
ATTN: SPTD
ATTN: STSP
ATTN: DDST
3 cy ATTN: TITL Tech. Library

Commander, Field Command
Defense Nuclear Agency
ATTN: FCTMD
ATTN: FCPR

Director
Joint Strat. Tgt. Planning Staff, JCS
ATTN: JPTM
ATTN: JPTP
ATTN: JLTW-2
ATTN: JPST

Chief
Livermore Division, Field Command, DNA
Lawrence Livermore Laboratory
ATTN: FCPRL

OJCS/J-5
ATTN: J-5 Plans & Policy Nuc. Div.

Studies Analysis and Gaming Agency
ATTN: SDEB

Under Secretary of Def. for Rsch. & Engrg.
ATTN: S&SS (OS)

DEPARTMENT OF THE ARMY

Director
BMD Advanced Tech. Ctr.
Huntsville Office
ATTN: ATC-T, Melvin T. Capps
ATTN: Marcus Whitfield
ATTN: CRDABH-S, William C. Loomis

Program Manager
BMD Program Office
ATTN: DACS-BMZ
ATTN: DACS-BMT, John Shea
ATTN: DACS-BMT, Clifford E. McLain
ATTN: DACS-BMZ-D, Julian Davidson
ATTN: Technology Division

DEPARTMENT OF THE ARMY (Continued)

Commander
BMD System Command
ATTN: BDMSC-TEN, Noah J. Hurst
ATTN: BDMSC-TEB, R. Simpson

Dep. Chief of Staff for Rsch. Dev. & Acq.
ATTN: NCB Division

Deputy Chief of Staff for Ops. & Plans
ATTN: Dir. of Nuc. Plans & Policy

Commander
Harry Diamond Laboratories
ATTN: DRXDO-RBH, James H. Gwaltney
ATTN: DRXDO-TF, Robert B. Oswald, Jr./ D. Schallhorn
ATTN: DRXDO-NP, Francis N. Wimenitz

Commander
Picatinny Arsenal
ATTN: SARPA-FR-E, Louis Avrami
ATTN: SARPA-ND-C-T, Donald Miller

Director
U.S. Army Ballistic Research Labs
ATTN: J. H. Keefer, DRDAR-BLE
ATTN: William J. Schuman, Jr., DRXRD-BVL
ATTN: J. T. Frasier, DRXBR-TB
ATTN: Julius J. Meszaros, DRXBR-X

Commander
U.S. Army Mat. & Mechanics Rsch. Ctr.
ATTN: DRXMR-HH, John F. Dignam

Commander
U.S. Army Materiel Dev. & Readiness Cmd.
ATTN: DRCDE-D, Lawrence Flynn

Commander
U.S. Army Missile Command
ATTN: DRS-RKP, W. B. Thomas

Chief
U.S. Army Research Office
ATTN: Technical Library

DEPARTMENT OF THE NAVY

Chief of Naval Material
ATTN: MAT 0323, Irving Jaffe

Chief of Naval Operations
ATTN: Op 981

Chief of Naval Research
ATTN: Code 464, Thomas P. Quinn

Director
Naval Research Laboratory
ATTN: Code 5180, Mario A. Persechino
ATTN: Code 2600, Tech. Lib.
ATTN: Code 7770, Gerald Cooperstein

DEPARTMENT OF THE NAVY (Continued)

Commander
Naval Sea Systems Command
ATTN: 0333A, Marlin A. Kinna
ATTN: Code 0351

Officer-In-Charge
Naval Surface Weapons Center
ATTN: Code WA501, Navy Nuc. Prgms. Off.
ATTN: Code WA07, Carson Lyons
ATTN: Code 2302

Commanding Officer
Naval Weapons Evaluation Facility
ATTN: Peter Hughes

Director
Strategic Systems Project Office
ATTN: NSP-272
ATTN: NSP-273

DEPARTMENT OF THE AIR FORCE

AF Materials Laboratory, AFSC
ATTN: MBC, Donald L. Schmidt
ATTN: T. Nicholas
ATTN: MBE, George F. Schmitt
ATTN: MAS

AF Rocket Propulsion Laboratory, AFSC
ATTN: RTSN, G. A. Beale

AF Weapons Laboratory, AFSC
ATTN: DYV
ATTN: DYT
ATTN: DYS
ATTN: SUL
ATTN: NT

Headquarters
Air Force Systems Command
ATTN: SOSS
ATTN: XRTO

Commander
Foreign Technology Division, AFSC
ATTN: TDPTN
ATTN: TDFBD, J. D. Pumphrey
ATTN: PCBG

Hq. USAF/RD
ATTN: RDQSM
ATTN: RD

SAMSO/DY
ATTN: DYS

SAMSO/MN
ATTN: MNNR

SAMSO/RS
ATTN: RSMA
ATTN: RSS
ATTN: RSSE

Commander in Chief
Strategic Air Command
ATTN: XOBM
ATTN: XPFS
ATTN: NRI
ATTN: XPQM
ATTN: DOXT

DEPARTMENT OF THE AIR FORCE (Continued)

AFTAC
ATTN: Col. Earnest F. Dukes, Jr.

DEPARTMENT OF ENERGY

Division of Military Application
Department of Energy
ATTN: Doc. Con. for Res. & Dev. Branch

University of California
Lawrence Livermore Laboratory
ATTN: Joseph E. Keller, Jr., L-125
ATTN: C. Joseph Taylor, L-92
ATTN: Larry W. Woodruff, L-96
ATTN: D. Hanner

Los Alamos Scientific Laboratory
ATTN: Doc. Con. for Robert Skaggs
ATTN: Doc. Con. for R. Dingus
ATTN: Doc. Con. for John McQueen/
J. W. Taylor
ATTN: Doc. Con. for D. Shover

Sandia Laboratories
Livermore Laboratory
ATTN: Doc. Con. for 8131, W. F. Norris, Jr.
ATTN: Raymond Ng
ATTN: Doc. Con. for T. Gold

Sandia Laboratories
ATTN: Doc. Con. for R. R. Boade
ATTN: Doc. Con. for Clarence Mehl
ATTN: Doc. Con. for Jerry Kennedy
ATTN: Doc. Con. for Carter Broyles

DEPARTMENT OF DEFENSE CONTRACTORS

Acurex Corporation
ATTN: J. Huntington

Aerospace Corporation
ATTN: Robert L. Strickler
ATTN: Richard Crolius, A2-Rm. 1027
ATTN: R. Mortensen
ATTN: W. Barry

Avco Research & Systems Group
ATTN: John E. Stevens, J100
ATTN: Doc. Control
ATTN: John Gilmore, J400
ATTN: William Broding
ATTN: P. Grady

Battelle Memorial Institute
ATTN: Merwyn R. Vanderlind

The Boeing Company
ATTN: Brian Lempriere

California Research & Technology Inc.
ATTN: Ken Kreyenhagen

Effects Technology, Inc.
ATTN: Robert Wengler/F. S. Bick
ATTN: Richard Parisse/H. Rosen

Ford Aerospace & Communications Operations
ATTN: P. Spangler

DEPARTMENT OF DEFENSE CONTRACTORS (Continued)

General Electric Company
Space Division
Valley Forge Space Center
ATTN: Daniel Edelman
ATTN: G. Harrison

General Electric Company
TEMPO-Center for Advanced Studies
ATTN: DASIAC

General Research Corporation
ATTN: Robert E. Rosenthal

Institute for Defense Analyses
ATTN: Joel Bengston
ATTN: IDA Librarian, Ruth S. Smith

ION Physics Corporation
ATTN: Robert D. Evans

Kaman Avidyne
Division of Kaman Sciences Corp.
ATTN: Ray Reutinick

Kaman Sciences Corporation
ATTN: Thomas Meagher
ATTN: Donald C. Sachs/R. O'Keefe
ATTN: Frank H. Shelton

Ktech Corporation
ATTN: N. H. Froula

Lockheed Missiles & Space Co., Inc.
ATTN: Oliver Burford, Dept. 81-14
ATTN: Richard Walls, Dept. 81-14

Lockheed Missiles & Space Co., Inc.
ATTN: T. R. Fortune

Martin Marietta Corporation
Orlando Division
ATTN: Laird Kinnaird

McDonnell Douglas Corporation
ATTN: H. M. Berkowitz
ATTN: L. Cohen
ATTN: J. Kirby
ATTN: J. Peck

Pacific-Sierra Research Corp.
ATTN: Gary Lang

Physics International Company
ATTN: Doc. Con. for James Shea

Prototype Development Associates, Inc.
ATTN: John McDonald/T. McKinley
ATTN: Neal Harington

R&D Associates
ATTN: F. A. Field
ATTN: Paul Rausch

The Rand Corporation
ATTN: R. Robert Rapp

DEPARTMENT OF DEFENSE CONTRACTORS (Continued)

Science Applications, Inc.
ATTN: Olan Nance

Science Applications, Inc.
ATTN: William M. Layson

Southern Research Institute
ATTN: C. D. Pears

SRI International
ATTN: Herbert E. Lindberg
ATTN: George R. Abrahamson
ATTN: Donald Curran

Systems, Science & Software, Inc.
ATTN: Russell E. Duff
ATTN: G. A. Gurtman

Terra Tek, Inc.
ATTN: Sidney Green

SRI International
ATTN: Harold Carey

TRW Defense & Space Sys. Group
ATTN: W. W. Wood
ATTN: J. Farrell
2 cy ATTN: Peter K. Dai, R1/2170/D. Jortner

TRW Defense & Space Sys. Group
San Bernardino Operations
ATTN: William Polich